Porous Poly(lactic acid) and PLA-Nanocomposite Structures

Xia Liao,[1,2] Arghavan V. Nawaby,[2] Hani E. Naguib[1]

[1]*Department of Mechanical and Industrial Engineering, University of Toronto, Toronto, Canada M5S 3G8*
[2]*Institute for Chemical Process and Environmental Technology, National Research Council of Canada, Ottawa, Canada K1A 0R6*

Received 23 February 2011; accepted 27 May 2011
DOI 10.1002/app.34994
Published online 5 October 2011 in Wiley Online Library (wileyonlinelibrary.com).

ABSTRACT: This article presents foaming behaviors and cellular structures of poly(lactic acid) (PLA)-clay nanocomposite and respective neat PLA foams using CO_2 as a foaming agent. The effects of nanoclay and foaming conditions on the foam morphology and mechanical properties of neat (PLA) and PLA-clay nanocomposites have been investigated by temperature modulated differential scanning calorimeter (TMDSC), X-ray diffraction, scanning electron microscopy, and tensile properties. CO_2-induced crystallization in PLA and PLA-clay nanocomposites and the crystallinity increased with an increase in saturation time. The present of clay acted as nucleation site to facilitate the crystallization process of PLA thus resulted in smaller crystallites and lower crystallinity. Unique skin-core foam morphologies in PLA and PLA-clay nanocomposites were obtained by controlling the crystallinity. Clay nanoparticles served as nucleation sites to generate foam morphology in PLA-clay sample with high crystallinity. The introduction of the cellular structure improved the mechanical strength of the material and the specific strength of PLA foams were increased in the presence of a small amount of MMT. © 2011 Wiley Periodicals, Inc. J Appl Polym Sci 124: 585–594, 2012

Key words: poly(lactic acid); nanocomposite; foam; CO_2

INTRODUCTION

Petrochemical-based polymers have been widely used in the past half century and have brought many benefits to mankind. However, since synthetic polymers do not readily decompose, the persistent plastic wastes are becoming a global environmental problem. On the other hand, the petroleum resources are finite and becoming limited. Therefore, it is urgent to develop renewable source based environmental benign plastic materials with excellent properties, especially in short-term packaging and disposable applications which would not involve the use of toxic components in the manufacture processing and could degrade naturally. One of the most promising polymers is poly (lactic acid) (PLA) because it is made from agriculture products and is readily biodegradable.[1] However, the strength, thermal stability, gas barrier, solvent resistance, and flame retardance of pure PLA is not enough for the end use. Formation of composites using inorganic or natural fillers is one of the effective ways to improve material performance and extend further applications.

Correspondence to: H. E. Naguib (naguib@mie.utoronto.ca).

Journal of Applied Polymer Science, Vol. 124, 585–594 (2012)

Polymer composites are widely used in automotive, aerospace, construction and electronic industries since they exhibit improved mechanical properties and physical properties. Of particular interest is polymer nanocomposites based on organically modified layered silicate (OMLS) because of their significant improved properties as compared with the neat polymer by adding a small amount of nanoparticles.[2–5]

Polymeric foams have been widely used in a variety of industries because of the excellent properties such as lighter weight, high strength/weight ratio, superior insulating abilities, and energy absorbing performance.[6] However, the foam applications are limited by their inferior mechanical strength, poor surface equality, and low thermal and dimensional stability. Carbon dioxide as an environmentally friendly solvent has found many applications in polymer synthesis and processing. Using CO_2 as a physical blowing agent in the fabrication of microcellular foams has received significant attention in the past decade.[7–9] A small amount of well-dispersed nanoparticles in polymer may act as nucleation sites to facilitate the cell nucleation process using CO_2 as a foaming agent, via batch process[10,11] or by direct extrusion.[12] Compared with the neat polymer foams, nanocomposite foams may show improved cell morphology resulting in enhanced thermomechanical properties.

While numerous studies are available on the foaming of polymer, comparatively very limited work has been done regarding the foaming of a biodegradable polymer-layered silicate nanocomposite. Okamoto et al. prepared PLA-clay nanocomposite foams in a batch process by using supercritical CO_2 as a physical foaming agent.[13–16] The foams exhibited closed cell structure with homogeneous cells from microcellular to nanocellular in the case of nanocomposites, while the neat PLA foam showed nonuniform cell structure with large cell size. Nanocomposite foams showed a smaller pore size and larger pore density compared with neat PLA foam, suggesting that the dispersed silicate particles act as nucleating sites for cell formation. PLA is a semicrystalline polymer and crystallization of PLA induced by CO_2 has been observed.[17,18] The presence of crystalline regions complicates the foaming process. Since CO_2 gas does not dissolve in crystallites, the bubble nucleation is nonhomogeneous, resulting in difficulties controlling the cellular morphology of polymers with a high degree of crystallinity. Compared with amorphous polymer-gas system, relatively high temperature is required to produce microcellular foam in a semicrystalline polymer.[19] Semicrystalline poly(L-lactic acid) (PLLA) did not form porous matrices when saturated in CO_2 at 5.5 MPa and 25°C using pressure quenching method, while amorphous poly(D,L-lactic acid) (PDLLA) exhibited a foamed structure with porosity up to 95%.[20,21] Nonuniform close-pore structures ($\sim$ 230 μm) in semicrystalline PLA were obtained when sample saturated in CO_2 at 140°C and 10 MPa for 2 h, and subsequently foamed just below the melt temperature (T_m = 168°C) of the matrix at 165°C.[15,16] Other report on producing PLA foams in CO_2 also conducted at high temperatures (100–140°C) and high pressures (14–30 MPa).[13,14]

In a batch foaming process, materials are first saturated with an inert gas at certain temperatures and pressures to form a homogeneous polymer-gas solution. The polymer-gas mixture subsequently quenched into a supersaturated state either by reduced pressure or increased temperature. If the temperature is higher than the glass transition temperature, T_g, of the polymer-gas system, the release of pressure would result in supersaturation and cell nucleation and growth occurred. When the saturation temperature is lower than the T_g of polymer-gas system, gas bubble is not able to nucleate and grow after the release of pressure because of the high rigidity of the polymer chains. Foaming may occur when temperature is raised above T_g. Batch foaming is generally carried out at temperatures lower than the polymer flowing temperature. Therefore, the saturation time of batch foaming normally is from hours to days depending on diffusivity of CO_2 in polymer matrix, which significantly limits the productivity. This article provides a simple and efficient method to produce various types of PLA and PLA-clay nanocomposites morphologies in a few minutes at subcritical conditions by controlling the physical properties of polymer in CO_2. The effect of clay on the crystallization induced in CO_2 and the foam morphology as a function of CO_2 saturation time and foaming temperature are investigated.

EXPERIMENTAL

Materials

PLA with a D-content 1.1%–1.7% and its nanocomposites with 2 wt % organically modified nanoclay were kindly supplied by Unitika, Japan.

Samples in sheets about 400 μm thick were prepared by compression molding at 190°C followed by quenching in ice water.

Characterization

Gas solubility measurements

Sorption kinetic studies were carried out using a CAHN D110 microbalance. The detailed description of this gravimetric technique has been reported elsewhere.[22] Equilibrium solubility data was obtained by correcting all the data for balance zero shift and buoyancy effect due to dilation in polymer. The sorption curves where then modeled using hybrid method and diffusion coefficients of CO_2 in PLLA were estimated.

CO_2 induced crystallization

The thermal behaviors of PLA and its nanocomposites were characterized by a temperature modulated differential scanning calorimeter (TMDSC, TA2920, TA instruments). Measurements were performed under nitrogen at a heating rate of 5°C/min with a heating/cooling cycle of the modulation period 60 s and the amplitude of ± 0.796°C. Due to the recrystallization of polymer during DSC heating process, the extra heat absorbed by the newly formed crystallites has to be subtracted from the total endothermic heat flow to measure the crystallinity, χ_c, of polymer. As shown in Figure 1, the total heat flow using TMDSC technique is separated into reversing signal (i.e., the glass transition, melting) and nonreversing component (i.e., crystallization, crystal perfection and reorganization, cure, and decomposition). The endothermic heat flow ΔH of the initially existing crystallites can be calculated as $\Delta H = \Delta H_{\text{rev}} - \Delta H_{\text{nonrev}}$, where ΔH_{rev} is the melting enthalpy from the reversing heat flow profile and ΔH_{nonrev} is the crystallization enthalpy from the nonreversing heat

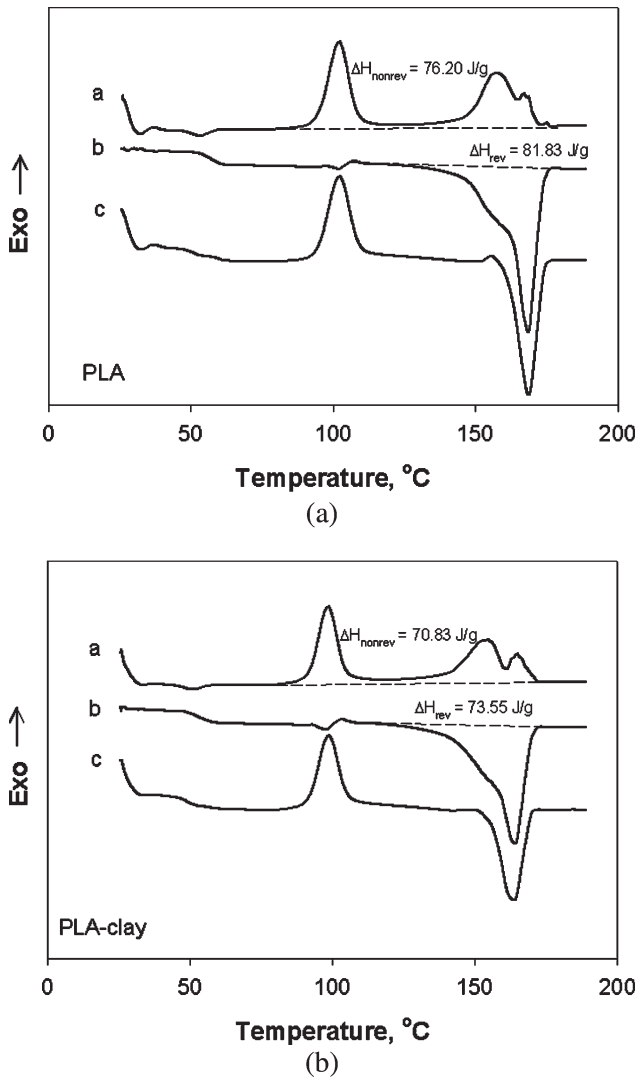

Figure 1 TMDSC curves for PLA and PLA-clay: (a) nonreversing heat flow and (b) reversing heat flow.

flow profile. The crystallinity of PLA and PLA-clay samples was thus calculated as $\chi_c = \Delta H/\Delta H^\circ$ with $\Delta H^\circ = 93$ J/g, which is the melting enthalpy of 100% crystalline poly (L-lactic acid).[23] The crystallinity data obtained from TMDSC were compared with the ones from x-ray results.

The structure of PLA-clay nanocomposites and the effect of CO_2 on the crystallization of PLA and its nanocomposite were also investigated by a Bruker GADDS diffraction system with Co K_α and a two-dimensional HISTAR detector. Polymer sheets were saturated with CO_2 at 25°C and 5.5 MPa for different time intervals in a saturation vessel. The pressure in the vessel was released rapidly and samples were aged for at least 5 days prior to obtaining X-ray diffraction patterns. Samples were analyzed in transmission mode with a 1 mm monocapillary optic and a collimator-mounted beamstop. The background scatter was subtracted from the collected frames after accounting for the attenuation of the scattering by the sample using $I/I_o = te^{(-\mu t)}$; where t is the sample thickness and μ is the linear absorption coefficient. The crystalline volume fractions were then determined by comparing the relative areas under the crystalline peaks to that associated with the amorphous material.

Foaming and foam characterization

Foamed specimens were prepared by saturating PLLA samples with CO_2 at 25°C and 5.5 MPa for different saturation times. The samples were then foamed in the temperature range 50 to 100°C. Foam morphologies were analyzed using JEOL JSM 840A field emission scanning electron microscopy. The foam density was measured by weighing the sample in air and in water using an electronic balance with a resolution of ±10 μg.

Mechanical testing

The tensile mechanical properties were tested with an Instron 5565 machine with a 500*N* load cell and a crosshead speed of 10 mm/min at room temperature (23°C). Rectangular strip samples were used. The Young's modulus was obtained by calculating the maximum slope at the initial elastic portion of the stress–strain curves. Five specimens were tested for each data point and the averages were reported.

RESULTS AND DISCUSSION

CO_2 induced crystallization

The DSC thermograms of PLA and its nanocomposites are shown in Figure 1. The cold crystallinzation temperature (T_c) of quenched PLA and its nanocomposites is 102.1°C and 98.4°C, respectively. The nanosized layered plates provided large surface area due to their small size and thus the clay particles could act as effective nucleating sites of PLA crystallization. The increased nucleating sites are likely to facilitate the PLA crystallization process in the nanocomposites, and thus T_c is decreased by the addition of nanoclays.

It has been found that CO_2 induced swelling and consequently increased the mobility of polymer chains and lowered T_g at the same time. Therefore, the reorientation of the chains to a lower free-energy crystalline structure is thermodynamically favorable which resulted in crystallinity at a lower temperature. The crystallization in PLA and PLA-clay samples was observed after saturated with CO_2 at 5.5 MPa and 25°C for 1 min and the crystallinity increased with increasing saturation time as showed in Figure 2. PLA-clay samples exhibited a lower

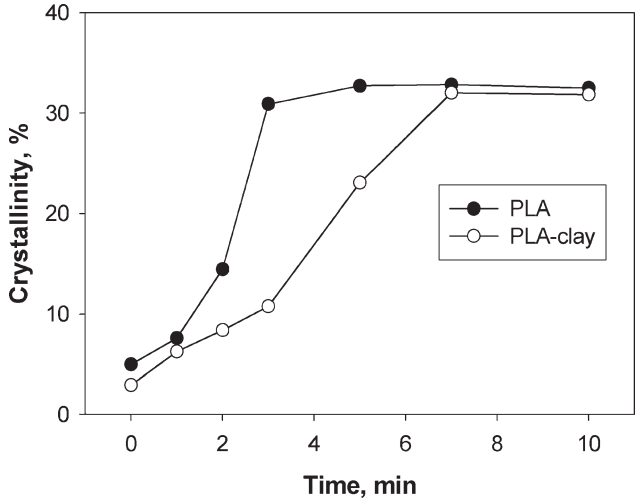

Figure 2 Crystallinity of PLA and PLA-clay saturated in CO_2 at 5.5 MPa and 25°C for different time.

crystallinity and melting temperatures (T_m) (Table I) than PLA saturated in CO_2 at the same conditions. Nam et al.[24] and Ray et al.[25] reported the effect of clay particles on the crystallite structure, morphology, and crystallization kinetics of pure PLA. The decrease of spherulitic size with addition of organically modified montmorillonite (MMT) is observed. The overall crystallization rate and spherulitic texture of pure PLA were strongly influenced in the presence of MMT particles at atmosphere.[24] The dispersed clay particles act as a nucleating agent, which is evident from the increase in the number of density of nuclei causing smaller spherulite formation. More nucleation sites would lead to large numbers of small crystallites, which resulted in a lower degree of overall crystallinity.[26,27] Therefore, the lower melting temperature and crystallinity of PLA nanocomposite treated with CO_2 is probably because the incorporated nanoclay increased the number of small crystallites and subsequently lower the overall crystallinity of PLA.

Figure 3 shows the x-ray patterns for PLA and PLA-clay nanocomposites samples saturated with CO_2 gas at 5.5 MPa and 25°C for 1, 2, 3, 5, 7, and 10 min, respectively. The presence of CO_2 did not change the crystalline structure of PLA and PLA-clay nanocomposites. The diffraction peaks became narrower and stronger with increasing saturation time, which indicated the crystallinity increased. The width of diffraction peaks is related to the size of the ordered regions. The wide peak indicated that the crystal size of PLA-clay sample is smaller than PLA, which coincided with the DSC work.

It was found that the addition of small amount of clay significantly enhanced the biodegradability of neat PLA.[28,29] The well distributed clay particles in the polymer means parts of the matrix are in contact with the clay edge and surface, therefore polymer chains would degrade more rapidly. Moreover, the crystallinity is one factor which controls the biodegradability of PLA because of the amorphous phase is more easily to degrade than the crystalline phase.[30] The biodegradation takes place in the amorphous regions first, and then the reaction zone moves to crystalline region in most semicrystalline

TABLE I
The Melting Temperatures (T_m, °C) of PLA and PLA-Clay Samples Saturated in CO_2 at 5.5 MPa and 25°C for Different Time

	Untreated	1 min	2 min	3 min	5 min	7 min	10 min
PLA	168.7	168.8	168.1	168.0	168.5	167.9	167.8
PLA-clay	163.7	162.3	162.4	163.1	164.1	164.3	163.7

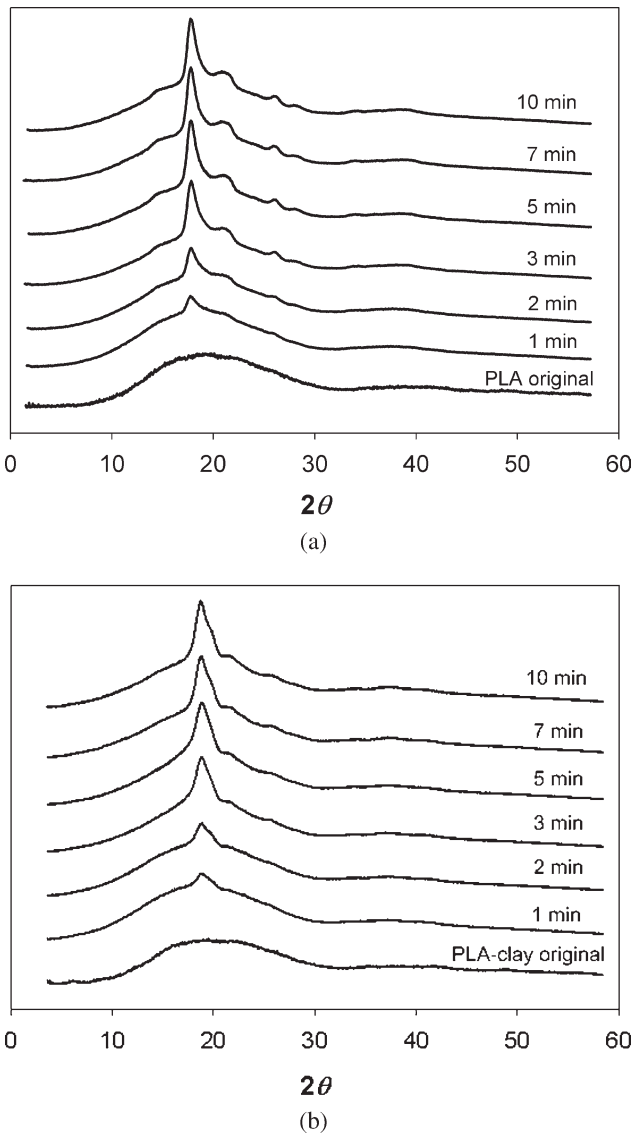

Figure 3 The X-ray diffraction patterns of (a) PLA and (b) PLA-clay saturated in CO_2 at 5.5 MPa and 25°C for different time.

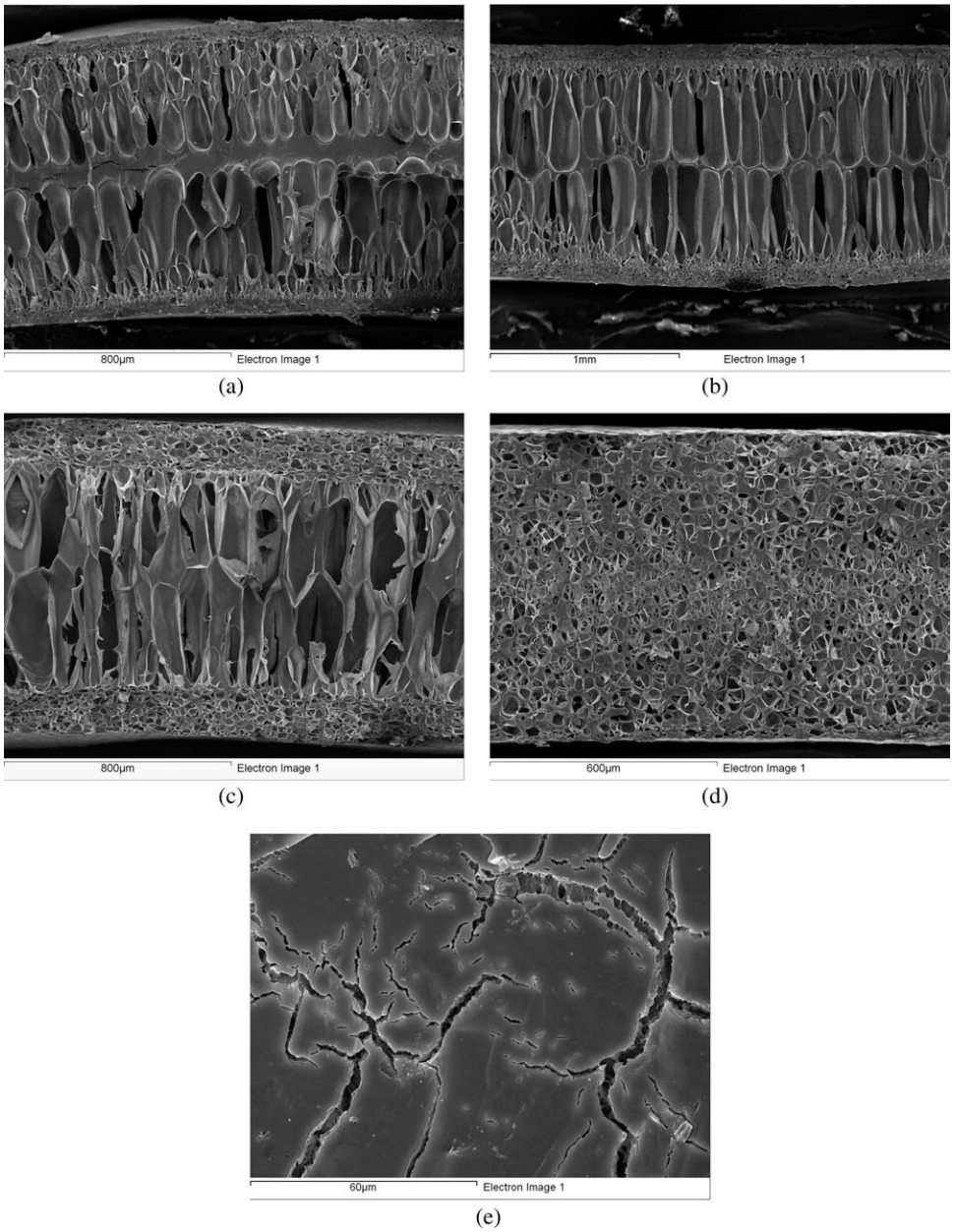

Figure 4 SEM microphotographs of PLA foams as a function of saturation time: (a) 1 min ×75, (b) 3min ×50, (c) 5 min ×75, (d) 7 min ×100, (e) 10 min ×1000 (samples saturated in CO_2 at 25°C and 5.5 MPa and subsequently foamed at 70°C).

polyester biodegradable polymer.[31] It is reasonable to assume that the biodegradation rate of the PLA-clay foams is faster than neat PLA foams because the smaller crystal size and lower crystallinity in nanocomposites after CO_2 treatment.

Foam morphology

The effect of CO_2 saturation time and foaming temperature on the formation of cellular morphologies in PLA and PLA-clay nanocomposite samples were investigated. A skin-core structure was observed in PLA [Fig. 4(a)] and its nanocomposite [Fig. 5(a)] contacted with CO_2 at 5.5 MPa and 25°C for 1 min and subsequently foamed at 70°C. Such unique foam morphology also has been observed in PLLA-CO_2 system and suggested to be contributed to limited degree of gas diffusion occurs in the sample with shorter contact times.[17] With increasing contact time to 3 min, the unfoamed area in the middle of samples decreased [Figs. 4(b) and 5(b)]. Samples contact with CO_2 for 5 min maintained the skin-core structure while the unfoamed area in the middle of samples disappeared [Figs. 4(c) and 5(c)]. With an increase the contact time to 7 min, PLA sample exhibited uniform interconnected foam morphology

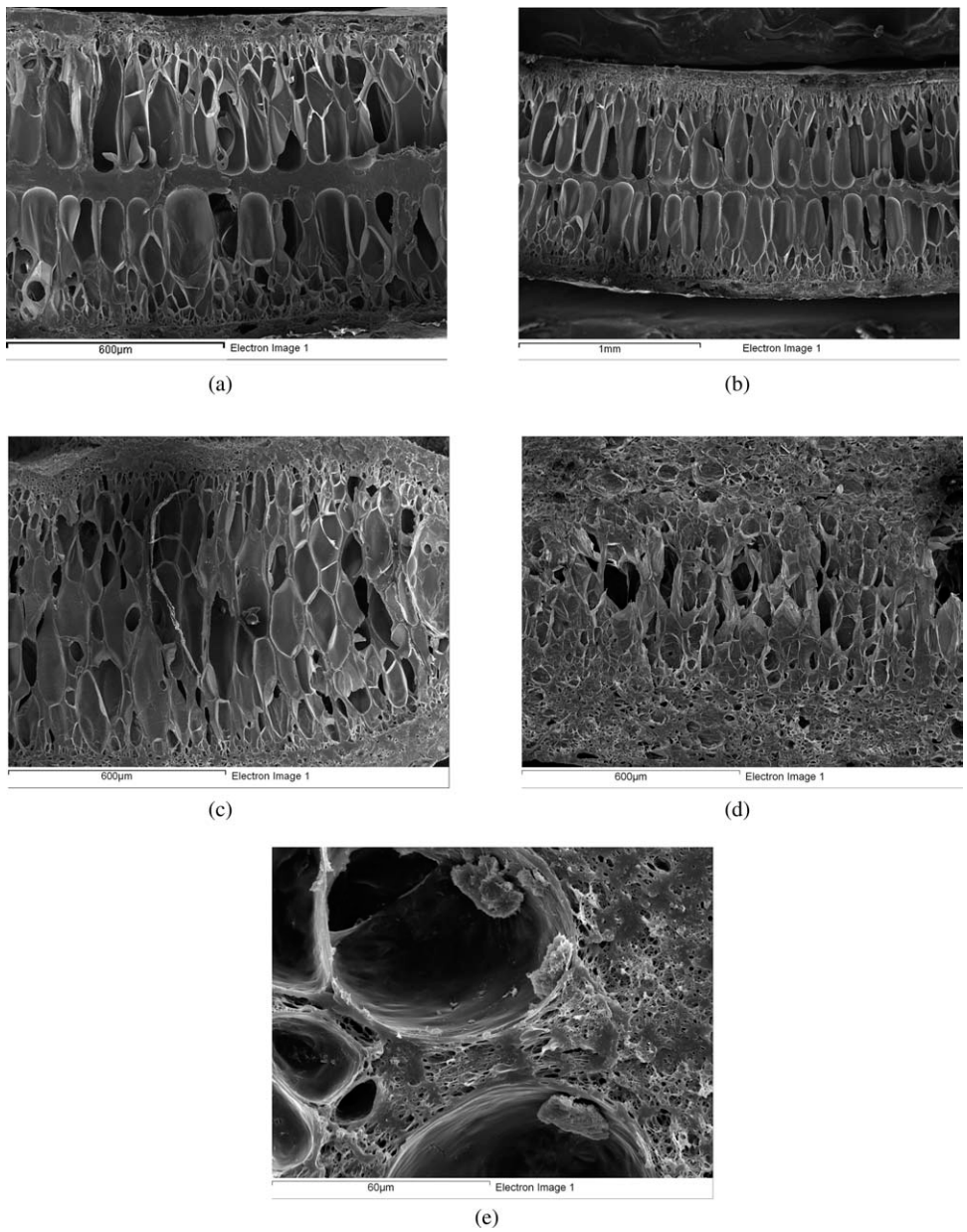

Figure 5 SEM microphotographs of PLA-clay foams as a function of saturation time: (a) 1 min ×100, (b) 3 min ×50, (c) 5 min ×100, (d) 7 min ×100, (e) 10 min ×1000 (samples saturated in CO_2 at 25°C and 5.5 MPa and subsequently foamed at 70°C).

[Fig. 4(d)], whereas the PLA-clay sample remained somewhat skin-core morphology [Fig. 5(d)]. Further increase the contact time to 10 min, only some gapes was obtained in PLA while the PLA-clay sample showed a foam structure with larger cell in the size range 20–80 μm and smaller cell in the size range 200–1500 nm.

The foam densities obtained as a function of CO_2 contact time are presented in Figure 6. The foam density in PLA-clay nanocomposite is lower than PLA at the same foaming condition, but a similar trend in foam density was observed. The foam density decreased with an increase in contact time and then increased after 7 min because the CO_2-induced crystallization resulted in foam difficulty.

Sorption data showed a maximum mass uptake of CO_2 in PLA and PLA-clay samples at 0.8–0.9 h at 5.5 MPa and subsequent decrease in CO_2 concentration with an increase in saturation time. The distinctive knee is a preliminary indication of crystallization and has been observed in PLLA[17] and poly(ethylene terephthalate) (PET).[32] The solubility increased with increasing time and then leveled off when reached equilibrium in an amorphous polymer. In general, the plasticization of polymer in CO_2 result in a lower T_g and a higher degree of molecular mobility

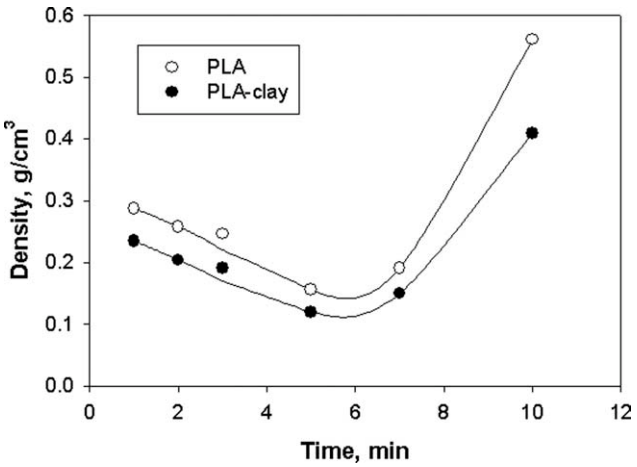

Figure 6 Foam density of PLA and PLA-clay as a function of saturation time (samples saturated in CO_2 at 25°C and 5.5 MPa and subsequently foamed at 70°C).

which allows the ordinarily rigid chains to rearrange into a more energetically favored state, thus forming crystallites. The decrease in CO_2 uptake indicates that during CO_2 dissolution the PLLA sheet rejects CO_2, which shows an indicative fact that CO_2 does not dissolve in the crystalline region of polymer. In an amorphous polymer, cell density and cell structure is dependent on the amount of gas dissolved. Higher solubility of gas in polymer can induce a larger cell population during the foaming process thus lower foam density is obtained. However, the foam density of PLA and PLA-clay samples increased after CO_2 saturation for 7 min, although the CO_2 solubility increased until 0.8–0.9 h. TMDSC data of PLA and PLA-clay nanocomposite samples saturated at 5.5 MPa revealed an increase in crystallinity with an increase in contact time and then level off (Fig. 2). This result indicated that the crystallization process is a vital factor in forming cellular morphologies. CO_2 induced crystallization has been found to play an important role in the foaming processing through its effects on the cell nucleation and growth mechanism. The effects of the crystallinity and crystal morphology on the foaming behavior and cellular structure of semicrystalline polymers such as syndiotactic polystyrene (SPS),[33] high density polyethylene (HDPE), polybutylene (PB), polypropylene (PP),[34] PET,[19,35,36] poly(ester amide) (PEA),[37] and HDPE/PP[38,39] have been studied. In general, higher cell densities and smaller cell sizes are obtained in semicrystalline polymers with low crystallinity, which are attributed to a significant contribution of heterogeneous nucleation at the amorphous/crystalline interfacial regions and the crystalline domains may serve as heterogeneous nucleation sites to produce gas bubbles.[35,36] However, the samples with high crystallinity are very difficult to get foam morphology. In microcellular process, foaming occurs when a thermodynamic instability is created in the polymer-gas solution. The foaming process includes three steps: cell nucleation, growth, and stabilization. The steps of cell growth and foam stabilization are related to the rheological properties of the polymer. The stiffness

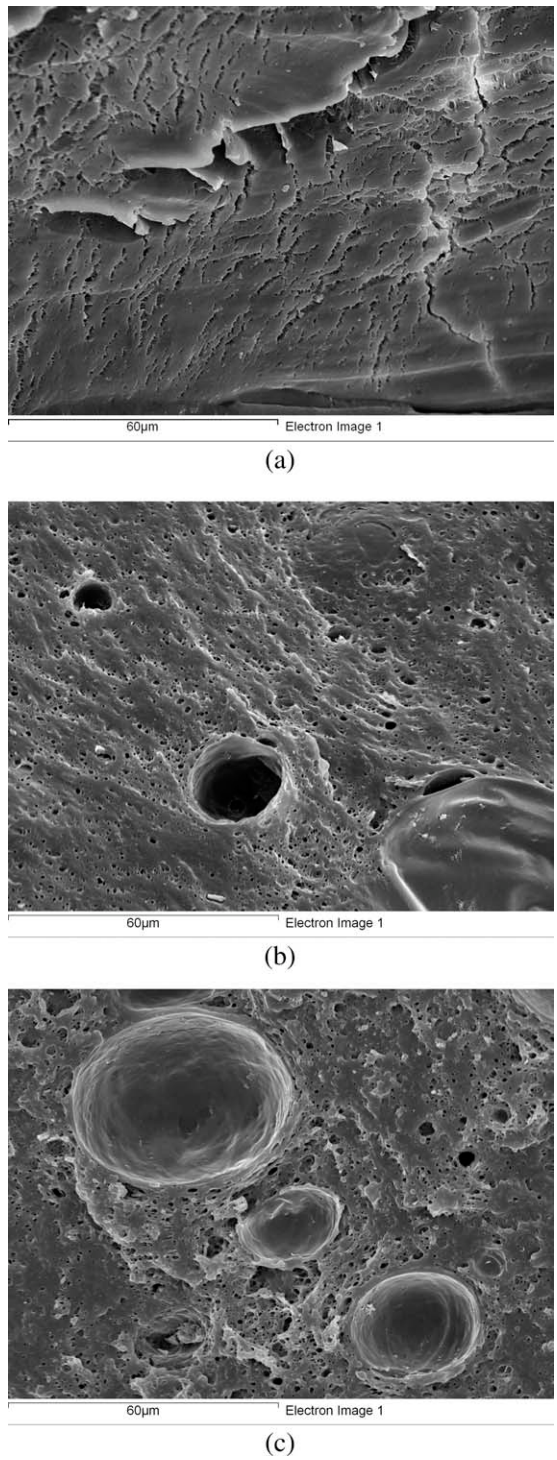

Figure 7 SEM microphotographs of PLA-clay foams as a function of foaming temperature: (a) 60°C ×1000, (b) 80°C ×1000, (c) 90°C ×1000 (samples saturated in CO_2 at 25°C and 5.5 MPa for 10 min).

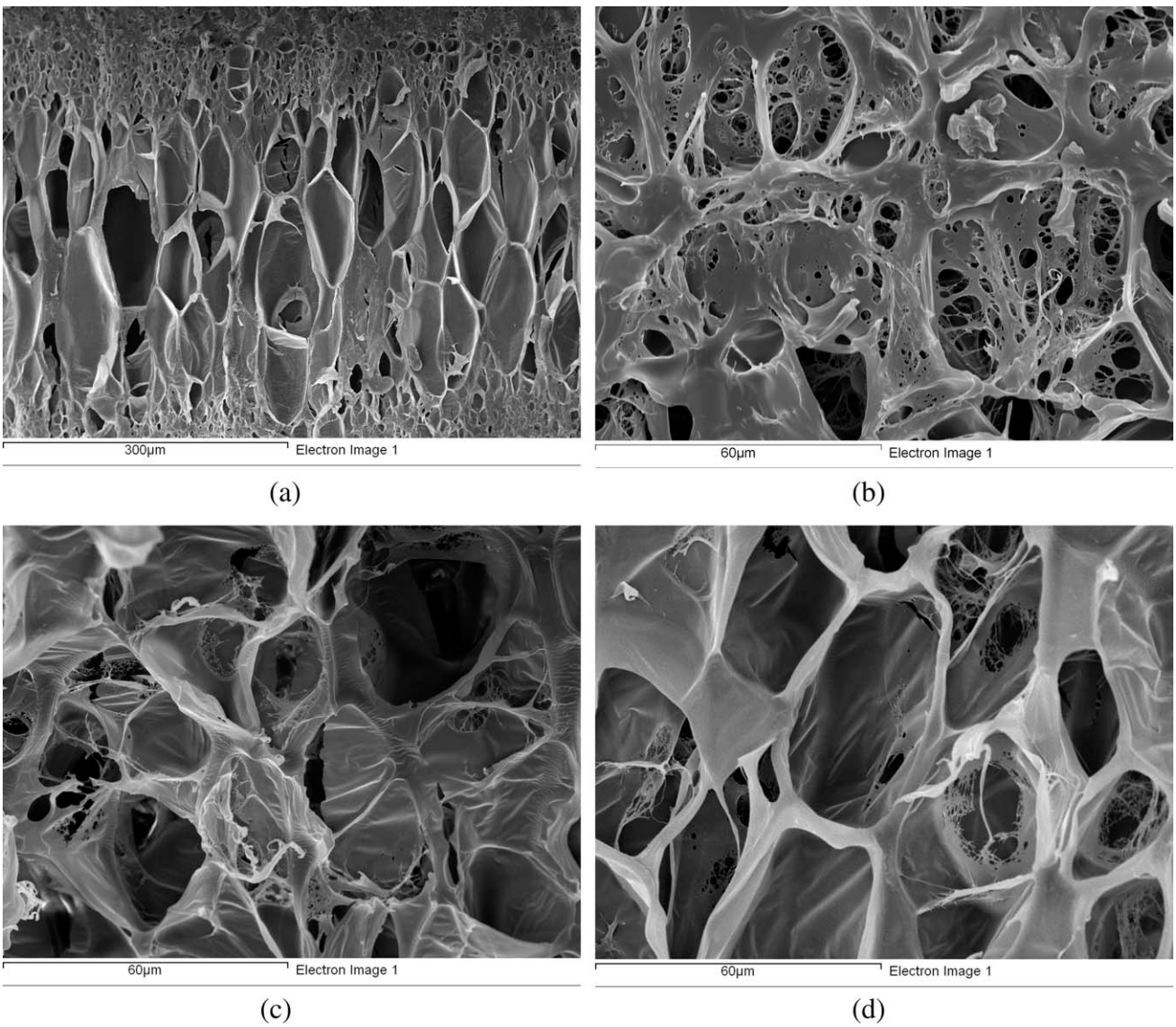

Figure 8 SEM microphotographs of PLA foams as a function of foaming temperature: (a) 60°C ×200, (b) 70°C ×1000, (c) 80°C ×1000, (d) 90°C ×1000 (samples saturated in CO_2 at 25°C and 5.5 MPa for 7 min).

of polymer matrix is controlled by the crystallinity and increase with increasing crystallinity.[34] The lack of foaming of PLA sample saturated for 10 min is probably related to the high ordered crystalline structure, which increases the modulus of polymer by several orders of magnitude.[19] Since the aspect ratio of clay particles is very high, the interaction between macromolecules and inorganic particles are enhanced to a great extent. Furthermore, the clay particles could serve as heterogeneous nucleation sites to greatly increase the formation of bubble nuclei.[40] According to the classical nucleation theory,[7,41,42] these heterogeneous nucleation agents provide a large interfacial area, thus reducing the nucleation energy during foaming process. Since the crystallinity of PLA and PLA-clay saturated for 10 min is almost the same, the foamed morphology obtained in PLA-clay sample is probably due to the nucleation sites of nanoclays.

Foaming temperature dependence of pore structure

PLA sample saturated at 5.5 MPa and 25°C for 10 min foamed from 60 to 90°C didn't exhibit foam morphology. However, the PLA-clay sample saturated 10 min subsequently foamed at 60°C produced a layered morphologies with cell size in the range 100–500 nm. For semicrystalline polymers, the pore growth is attributed to the viscoelastic behavior of the matrix. In this case, the primary factor effecting pore growth is the temperature dependent relaxation modulus. Increasing foam temperature leads to a decrease in the viscosity of polymer matrix and to

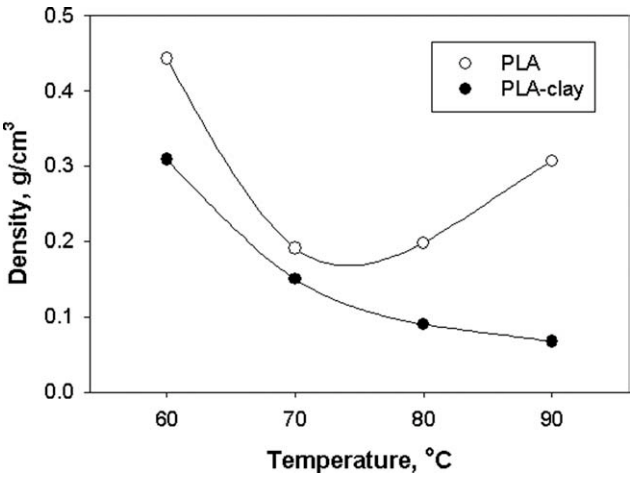

Figure 9 Foam density of PLA and PLA-clay as a function of foaming temperature (samples saturated in CO_2 at 25°C and 5.5 MPa for 7 min).

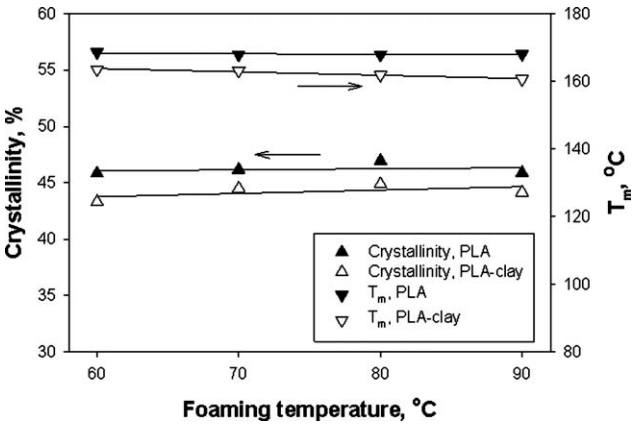

Figure 10 The crystallinity and melting temperatures of PLA and PLA-clay samples saturated in CO_2 at 5.5 MPa and 25°C for 7 min, and subsequently foamed at different temperatures.

an increase in the supersaturation, thus resulted in a higher cell density [Fig. 7(b,c)].

As shown in Figure 8(a), PLA sample saturated at 5.5 MPa and 25°C for 7 min and subsequently foamed at 60°C exhibited a skin-core structure. With increasing temperature to 70°C, the skin-core morphology disappeared, and a uniform foam structure with open cells was obtained. Further increase the temperature to 80 and 90°C resulted in foam morphologies with larger cells [Fig. 8(b,c)]. The dependence of foam density at different foaming temperatures is shown in Figure 9. The foam density of PLA-clay nanocomposite decreased with increasing the foaming temperature from 60 to 90°C, while the foam density of PLA decreased with an increase in temperature and then increased after 80°C. Since the crystallinity of PLA and PLA-clay samples didn't change with the foaming temperature as shown in Figure 10, the decrease in foam density of PLA at high temperature is contributed to the cell collapsed. The foam density decreased with increasing foaming temperature in PLA-clay foams is probably because the present of clay avoided the collapse of the foamed structure.

Mechanical test

The tensile properties of PLA and PLA/nanocomposite foams have been investigated. To normalize the impact of the foam density on the mechanical properties, specific strength, the tensile modulus divided by the relative density (the density of the foamed sample divided by the density of the virgin unfoamed sample), was used. As shown in Figure 11, the tensile modulus of PLA and PLA/nanocomposite sample decreased as a results of foaming because the less solid matrix available to support the load. However, the PLA and PLA-clay foamed samples saturated in CO_2 for different time exhibited higher specific strength than the unfoamed samples due to the cellular morphologies which could be supported by SEM results. PLA and PLA-clay foamed samples saturated for 5 min showed the highest specific strength. Compared with the nonfoamed samples, a weight reduction of 87 and 90% sacrifices the tensile modulus by 74 and 78% for PLA and PLA-clay foams, respectively. Therefore, the introduction of the cellular structure improved the mechanical strength of the material. The specific strength of PLA foams were increased in the presence of a small amount of MMT. As discussed earlier, the crystallinity of PLA -clay nanocomposites is lower than pristine PLA, but the specific strength increased by the incorporation of a small amount of nanosized clay. This observation suggested that the

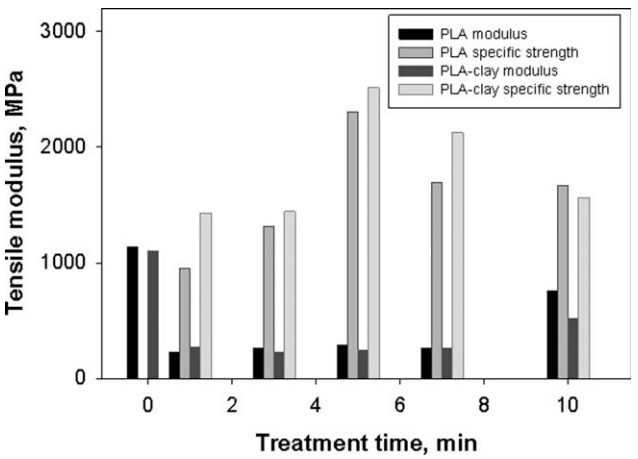

Figure 11 Tensile modulus of PLA and PLA-clay nanocomposites saturated in CO_2 at 5.5 MPa and 25°C for different time.

layered silicates of MMT act a mechanical reinforcement of polymer chains.[43]

CONCLUSIONS

Most microcellular polymer produced in a batch foaming process conducted at a high pressure and temperature for several hours or days. This article demonstrates that controlled unique foam morphologies can be generated in biodegradable PLA and PLA-clay nanocomposites by simply changed the CO_2 processing parameter at subcritical conditions in a short time. TMDSC and X-ray diffraction data revealed that CO_2 induced crystallization in PLA and PLA-clay nanocomposites and the crystallinity increased with an increase in saturation time. The presence of clay acted as nucleation site to facilitate the crystallization process of PLA thus resulted in smaller crystallites and lower crystallinity. The crystals induced in CO_2 plays a vital role in controlling the nucleation and growth of the cells during foaming process. Compared with the neat PLA foams, PLA-clay foams showed better specific tensile properties. We anticipate these unique microcellular PLA-clay foams with high biodegradation rate and good mechanical properties can have potential application in packaging industry.

The authors thank Mr. David Kingston and Mr. Floyd Toll for their assistance.

References

1. Drumright, R. E.; Gruber, P. R.; Henton, D. E. Adv Mater 2000, 12, 1841.
2. Sinha Ray, S.; Okamoto, M. Prog Polym Sci 2003, 28, 1539.
3. Biswas, M.; Sinha Ray, S. Adv Polym Sci 2001, 155, 167.
4. Alexander, M.; Dubois, P. Mater Sci Eng R 2000, 28, 1.
5. Giannelis, E. P.; Krishnamoorti, R.; Manias, E. Adv Polym Sci 1999, 138, 107.
6. Klempner, D.; Frisch, K. C. Handbook of Polymeric Foams and Foam Technology; Oxford University Press: New York, 1991.
7. Colton, J. S.; Suh, N. P. Polym Eng Sci 1987, 27, 493.
8. Goel, S. K.; Beckman, E. J Polym Eng Sci 1994, 34, 1137.
9. Arora, K. A.; Lesser, A. J.; McCarthy, T. J. Macromolecules 1998, 31, 4614.
10. Zeng, C. C.; Han, X. M.; Lee, L. J.; Koelling, K. W.; Tomasko, D. Adv Mater 2003, 15, 1743.
11. Nam, P. H.; Maiti, P.; Okamoto, M.; Kotaka, T.; Nakayama, T.; Takada, M.; Ohshima, M.; Usuki, A.; Hasegawa, N.; Okamoto, H. Polym Eng Sci 1907 2002, 42.
12. Henning Winter, H.; Gappert, G.; Ito, H. Macromolecules 2002, 35, 3325.
13. Ema, Y.; Ikeya, M.; Okamoto, M. Polymer 2006, 47, 5350.
14. Okamoto, M.; Nam, P. H.; Maiti, P.; Kotaka, T.; Nakayama, T.; Takada, M.; Ohshima, M.; Usuki, A.; Hasegawa, N.; Okamoto, H. Nano Lett 2001, 1, 503.
15. Ray, S. S.; Okamoto, M. Macromol Mater Eng 2003, 288, 936.
16. Fujimoto, Y.; Ray, S. S.; Okamoto, M.; Ogami, A.; Yamada, K.; Ueda, K. Macromol Rapid Commun 2003, 24, 457.
17. Liao, X.; Nawaby, A. V.; Whitfield, P.; Day, M.; Champagne, M.; Denault, J. Biomacromolecules 2006, 7, 2937.
18. Takada, M.; Hasegawa, S.; Ohshima, M. Polym Eng Sci 2004, 44, 186.
19. Baldwin, D. F.; Shimbo, M.; Suh, N. P. J Eng Mater Technol 1995, 117, 62.
20. Mooney, D. J.; Baldwin, D. F.; Suh, N. P.; Vacanti, J. P.; Langer, R. Biomaterials 1996, 17, 1417.
21. Sheridan, M. H.; Shea, D.; Peters, M. C.; Mooney, D. J. J Controlled Release 2000, 64, 91.
22. Wong, B.; Zhang, Z.; Handa, Y. P. J Polym Sci Part B: Polym Phys 1998, 36, 2025.
23. Fischer, E. W.; Sterzel, H. J.; Wegner, G.; Kolloid, Z. Z. Polymer 1973, 251, 980.
24. Nam, J Y.; Ray, S. S.; Okamoto, M. Macromolecules 2003, 36, 7126.
25. Ray, S. S.; Yamada, K.; Okamoto, M.; Fujimoto, Y.; Ogami, A.; Ueda, K. Polymer 2003, 44, 6633.
26. Park, C. S.; Lee, K. J.; Nam, J. D.; Kim, S. W. J Appl Polym Sci 2000, 78, 576.
27. Park, C. S.; Lee, K. J.; Kim, S. W.; Nam, J. D. J Appl Polym Sci 2002, 86, 478.
28. Ray, S. S.; Yamada, K.; Okamoto, M.; Ueda, K. Macromol Mater Eng 2003, 288, 203.
29. Ray, S. S.; Yamada, K.; Okamoto, M.; Ueda, K. Nano Lett 2002, 2, 1093.
30. Reeve, M. S.; McCarthy, S. P.; Downey, J. J.; Gross, R. A. Macromolecules 1994, 27, 825.
31. Doi, Y.; Jumagai, Y.; Tanahashi, N.; Nukui, K. Biodegradable Polymers and Plastics; Royal Society of Chemistry: London, 1992.
32. Brantley, N. H.; Kazarian, S. G.; Eckert, C. A. J Appl Polym Sci 2000, 77, 764.
33. Handa, Y. P.; Zhang, Z.; Nawaby, V.; Tan, J. Cell Polym 2001, 20, 241.
34. Doroudiani, S.; Park, C. B.; Kortschot, M. T. Polym Eng Sci 1996, 36, 2645.
35. Baldwin, D. F.; Park, C. B.; Suh, N. P. Polym Eng Sci 1996, 36, 1437.
36. Baldwin, D. F.; Park, C. B.; Suh, N. P. Polym Eng Sci 1996, 36, 1446.
37. Lips, P. A. M.; Velthoen, I. W.; Dijkstra, P. J.; Wessling, M.; Feijen, J. Polymer 2005, 46, 9396.
38. Rachtanapun, P.; Selke, S. E. M.; Matuana, L. M. J Appl Polym Sci 2003, 88, 2842.
39. Doroudiani, S.; Park, C. B.; Kortschot, M. T. Polym Eng Sci 1998, 38, 1205.
40. Ramesh, N. S.; Rasmussen, D. H.; Campbell, G. A. Polym Eng Sci 1994, 34, 1698.
41. Colton, J. S.; Suh, N. P. Polym Eng Sci 1987, 27, 485.
42. Colton, J. S.; Suh, N. P. Polym Eng Sci 1987, 27, 500.
43. Lee, J. H.; Park, T. G.; Park, H. S.; Lee, D. S.; Lee, Y. K.; Yoon, S. C.; Nam, J. D. Biomaterials 2003, 24, 2773.